

NUMERICAL SIMULATION OF DEFORMATION OF SAND BAR FORMED AT TIP OF FUTTSU CUSPATE FORELAND BY THE 2011 TSUNAMI

Akio Kobayashi¹, Takaaki Uda², Masumi Serizawa³, Shiho Miyahara³ and Masatoshi Endo¹

Futtsu Point is a cusped foreland separating Tokyo Bay and the Uraga Strait. On March 11, 2011, a tsunami generated by the Great East Japan Earthquake entered Tokyo Bay with approximately 2 m height, and flowed over this sand bar, dispersing the sand and leaving an isolated protruding sand bar. This resulted in the seawall at the foot of the sand bar being exposed to waves, increasing the potential for damage. After the tsunami, this isolated sand bar was significantly deformed, a sand spit was formed by the action of wind waves, and the seawall was refilled with sand. The subsequent shoreline changes of this protruding sand bar were measured, and the three-dimensional beach changes were calculated using the BG model (a three-dimensional model for predicting beach changes based on Bagnold's concept).

Keywords: Futtsu cusped foreland; beach changes; sand bar; Tsunami; BG model

INTRODUCTION

Futtsu Point is a cusped foreland separating Tokyo Bay and the Uraga Strait, with Futtsu and Shitazu fishing ports on the north and south sides of the slender cusped foreland, respectively, as shown in Fig. 1. Although this cusped foreland has long been stable, decreased sand supply from the south coast has resulted in erosion of the cusped foreland (Uda and Kanda, 1995), and the previously straight sand bar extending between Dai-ichikaiho island and the tip of the cusped foreland had become concave northward with several openings by February 3, 2011, as shown in Fig. 1. On March 11, 2011, a tsunami generated by the Great East Japan Earthquake entered Tokyo Bay with approximately 2 m height, and flowed over this sand bar, dispersing the sand and leaving an isolated protruding sand bar. This resulted in the seawall at the foot of the sand bar being exposed to waves, increasing the potential for damage. After the tsunami, this isolated sand bar was significantly deformed, a sand spit was formed by the action of wind waves, and the seawall was refilled with sand. The subsequent shoreline changes of this protruding sand bar were measured, and the three-dimensional beach changes were calculated using the BG model (a three-dimensional model for predicting beach changes based on Bagnold's concept) proposed by Serizawa and Uda (2011), and compared with the measured shoreline changes.

CHANGE IN SAND BAR OFFSHORE OF FUTTSU POINT BEFORE AND AFTER THE 2011 GREAT TSUNAMI

A large change at the tip of Futtsu Point was first discovered by a field observation on June 11, 2011. Because a tsunami of approximately 2 m height, which was recorded in the field observation at the south shore of Futtsu Point, hit the foreland on March 11, 2011, the sand bar at the tip of Futtsu Point was discharged by the overflow of this tsunami. Therefore, aerial photographs, as shown in Fig. 2, taken on February 3, 2011 before the tsunami and on March 27, 2012 after the tsunami were compared to study the impact of the tsunami. Before the tsunami, a slender, curved sand bar extended from the tip of Futtsu Point to Dai-ichikaiho island. On March 27, 2012, after the tsunami, almost all of the sand bar was disintegrated by the tsunami overflow, resulting in the submergence of the sand bar, and leaving a small sand bar at the tip of Futtsu Point. Comparing the broken line in Fig. 2(b), which shows the shape of the sand bar before the tsunami, and the shape of the submerged sand bar on March 27, 2012, it is revealed that the sand comprising the sand bar was transported northward, implying that the sand bar was flushed away by the northward flow of the tsunami. In addition, part of the sand was transported by the return flow near the tip of the cusped foreland.

METHOD OF FIELD OBSERVATION

A rectangular observation area was set up at the tip of Futtsu Point, as shown in Figs. 1 and 2, and the shoreline changes in this area were measured using a GPS between June 11, 2011 and October 16, 2012. The shoreline position was measured at the time when the tide level was approximately equal to

¹Department of Oceanic Architecture & Engineering, College of Science & Technology, Nihon University, 7-24-1 Narashinodai, Funabashi, Chiba 274-8501, Japan

²Public Works Research Center, 1-6-4 Taito, Taito, Tokyo 110-0016, Japan

³Coastal Engineering Laboratory Co., Ltd., 1-22-301 Wakaba, Shinjuku, Tokyo 160-001, Japan

the mean sea level. The changes in shoreline position were investigated using coordinates (x, y) with reference to a point in the vicinity of the seawall at the tip of Futtsu Point (Fig. 2). Swing-panorama photographs were also taken from the top of an observation tower, and a grain size analysis of the foreshore materials and measurements of the berm height and foreshore slope were carried out during low tide on February 26, 2012. The measured berm height was +0.97 m above the mean sea level and the foreshore slope was 1/8. Wave conditions were investigated using wave observation results offshore of Dainikaiho island located 2.4 km west of Dai-ichikaiho island, as shown in Fig. 1.



Figure 1. Location of study area at the tip of Futtsu Point and coordinate system.

(a) Feb. 3, 2011 (WL: +0.02m above MSL)



(b) March 27, 2012 (WL: +0.02m above MSL)

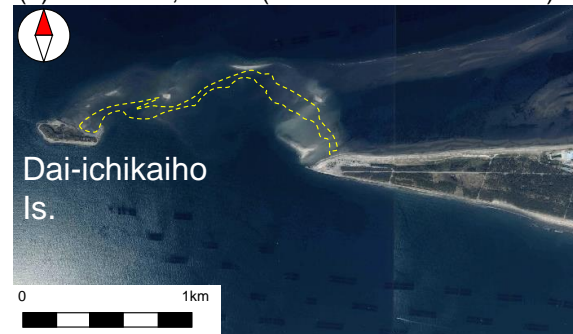


Figure 2. Aerial photographs of Futtsu Point taken on February 3, 2011 before the tsunami and March 27, 2012 after the tsunami.

RESULTS OF FIELD OBSERVATION

Wave conditions

Figure 3 shows the time change in daily maximum significant wave height $H_{1/3\max}$ and corresponding wave period $T_{1/3\max}$ between June 2011 and January 2012. Although the wave height normally ranges between 0.5 and 1 m, during typhoon or the passage of low pressure, the significant wave height increases as much as 1.5-2.0 m. The wave period is as short as 3-5 s in winter, and a long period wave of 10 s was also measured in summer.

The most important effect upon the deformation of the sand bar at the tip of Futtsu Point is caused by obliquely incident wind waves. Figure 4 shows the monthly changes in wave direction measured offshore of Dainikaiho island. Although the predominant wave direction in May and June is SSW or SW, the wave direction of NNW is predominant between July and October. Then, waves from SSW again predominate in November and December. From the morphology of the cusped foreland, waves incident from SSW do not affect the beach changes on the north side of the cusped foreland, as shown in Fig. 2, because Futtsu Point extends in the east-west direction, implying that the primary geomorphic agent of the deformation of the sand bar reduces waves incident from NNW.

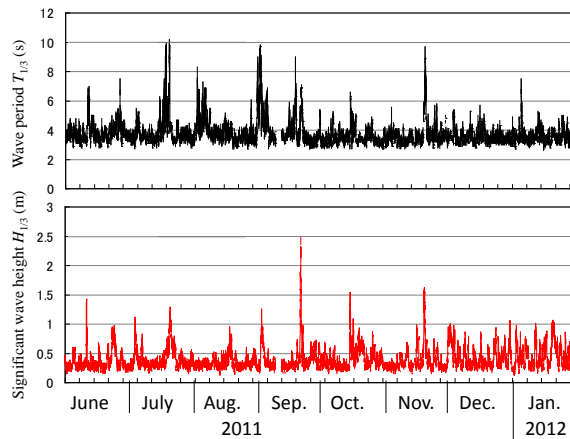


Figure 3. Change in significant wave height and period measured at Dainikaiho observatory between 2011 and 2012.

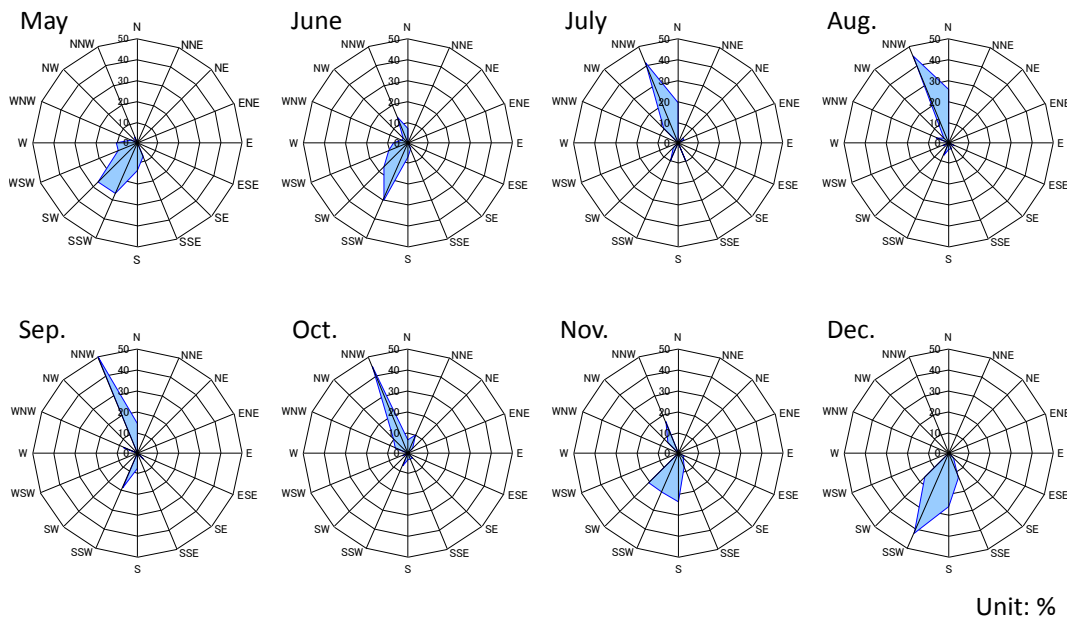


Figure 4. Seasonal changes in wave direction measured at Dainikaiho observatory between 2011 and 2012.

Site observation

On June 11, 2011, an overall picture of the newly formed sand bar was taken from an observation tower at the tip of Futtsu Point. Figure 5 shows an oblique photograph of a crescent-shaped sand bar formed on the north side. The shoreline on the west side of the sand bar was concave, whereas sand spit A was formed at the east end. On the concave shoreline near the west end of the sand bar, a large amount of shells were deposited on the shore face along the shoreline (Fig. 6). Figure 7 shows the deposition of shells at the northwest end of the sand bar, and the deposition pattern of shells, while forming many ridges on the foreshore, demonstrates that shells had been transported southward along the shoreline owing to the wave action during high tide. Beyond the northwest end of the sand bar, the

shoreline extended clockwise, as shown in Fig. 8, together with the deposition of a large amount of shells on the beach face. Figure 9 shows the concave shoreline and a sand spit mainly composed of shells, as denoted by arrow A in Fig. 5, where the formation of a sand spit was underway.

On the other hand, under the observation tower west of the newly formed sand bar, the beach was severely eroded, exposing the seawall to waves. Figure 10 shows the erosion behind the seawall. Fill materials behind the seawall were washed away by overtopped waves and a scarp was formed on the foot of pine trees.



Figure 5. Oblique photograph of a crescent-shaped sand bar.



Figure 6. Concave shoreline near west end of sand bar.



Figure 7. Deposition of shells at northwest end of sand bar.



Figure 8. Shoreline configuration beyond northwest end of the sand bar.



Figure 9. Concave shoreline and a sand spit mainly composed of shells.



Figure 10. Erosion behind seawall and scarp formation.

Swing-panorama photograph of sand bar

The observation using swing-panorama photographs from the observation tower was carried out between June 11, 2011 and October 16, 2012. Figure 11 shows the eight sets of photographs taken every two months with the reference points **a** and **b**, which were set at the location of the pine trees (**a**: right and **b**: left). The subsequent shoreline changes can be monitored by the change in the relative distance of the shoreline to points **a** and **b**.

On June 11, a slender sand bar extended westward (leftward) with a concave shoreline on the west side, and there was no sandy beach and the seawall was exposed to waves between points **a** and **b**, resulting in wave overtopping, and the seawall was partly destroyed, as already mentioned above. By

August 19, the tip of the sand bar had moved eastward (rightward in the figure) and the sand bar had markedly widened. However, no changes in the exposure of the seawall to waves between points **a** and **b** were observed. By October 26, the width of the sand bar markedly increased and a continuous shoreline extended westward, refilling the seawall between points **a** and **b** with sand. Until December 21, 2011, the sand bar further extended far west of point **b** while the seawall located at the southwest end was buried. The seawall at point **a** was buried under the sandy beach, whereas the sand bar was eroded out, implying that a marked change in the sand bar occurred within six months. After February 17, a smooth shoreline was formed.

Figure 12 shows the overall changes in the sand bar between June 11, 2011 and February 17, 2012. Up to June 11, when the observation began, a crescent-shaped sand bar of 130 m length had developed northward with a concave shoreline on the west side. By July 19, the tip of the sand bar had retreated. Then, because wind waves were incident from NNW in July, the west end of the sand bar was eroded, and the eroded sand was transported eastward, turning around the tip of the sand bar. By September 14, the sand bar had further inclined eastward, and a sand spit was formed on the east side until October 14. After October 14, the entire sand bar eroded out, reducing to a sand bar with a smooth shoreline, and diffusion-type shoreline changes occurred. By February 17, a gradually curved shoreline had formed and the seawall was protected by the recovered sandy beach.



Figure 11. Typical examples of swing-panorama photographs.



Figure 11. Typical examples of swing-panorama photographs (continued).

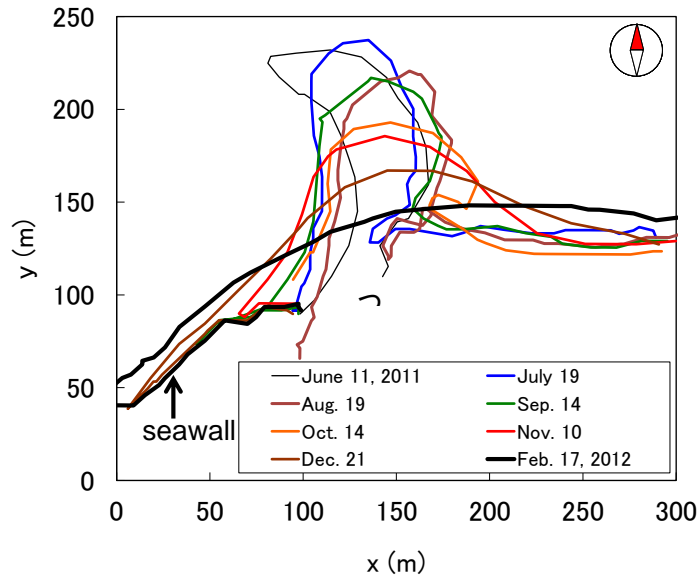


Figure 12. Overall changes in sand bar between June 11, 2011 and February 17, 2012.

NUMERICAL SIMULATION USING BG MODEL

Model

The BG model proposed by Serizawa and Uda (2011) with an additional term from Ozasa and Brampton (1980) was used in the numerical simulation. The fundamental equation is given by

$$\vec{q} = C_0 \frac{P}{\tan \beta_c} \left\{ \begin{array}{l} K_n \left(\tan \beta_c \vec{e}_w - |\cos \alpha| \nabla Z \right) \\ + \left\{ (K_s - K_n) \sin \alpha - \frac{K_2}{\tan \beta} \frac{\partial H}{\partial s} \right\} \tan \beta \vec{e}_s \end{array} \right\} \quad (-h_c \leq Z \leq h_R) \quad (1)$$

$$P = \rho u_m^3 \quad (2)$$

$$u_m = \frac{H}{2} \sqrt{\frac{g}{h}} \quad (3)$$

where $\vec{q} = (q_x, q_y)$ is the net sand transport flux, $Z(x, y, t)$ is the elevation with reference to the still water level, n and s are the local coordinates taken along the directions normal (shoreward) and parallel to the contour lines, $\nabla Z = (\partial Z / \partial x, \partial Z / \partial y)$ is the slope vector, e_w is the unit vector of the wave direction, e_s is the unit vector parallel to the contour lines, α is the angle between the wave direction and the direction normal to the contour lines, $\tan \beta = |\nabla Z|$ is the seabed slope, $\tan \beta_c$ is the equilibrium slope, $\tan \beta e_s = (-\partial Z / \partial y, \partial Z / \partial x)$, K_s and K_n are the coefficients of longshore and cross-shore sand transport, respectively, K_2 is the coefficient of the term given by Ozasa and Brampton (1980), $\partial H / \partial s = e_s \cdot \nabla H$ is the longshore gradient of the wave height H measured parallel to the contour lines, and $\tan \bar{\beta}$ is a characteristic slope of the breaker zone. In addition, C_0 is the coefficient transforming the immersed weight expression into the volumetric expression ($C_0 = 1 / \{(\rho_s - \rho)g(1 - p)\}$), where ρ is the density of seawater, ρ_s is the specific gravity of sand particles, p is the porosity of sand, and g is the acceleration of gravity), u_m is the amplitude of the seabed velocity due to the orbital motion of waves, h_c is the depth of closure, and h_R is the berm height.

$$h' = \left(\frac{h_R - Z}{h_R + h_0} \right)^r h_0 \quad (r=1) \quad (-h_0 \leq Z \leq h_R) \quad (4)$$

In addition, at locations higher than the berm height, the wave energy was set to be 0. The wave field was calculated every 10 steps of the calculation of topographic changes. In the numerical simulation of beach changes, the sand transport and continuity equations ($\partial Z / \partial t + \nabla \cdot \vec{q} = 0$) were solved on the x - y plane by the explicit finite-difference method.

In estimating the intensity of sand transport near the berm top and at the depth of closure, the intensity of sand transport was linearly reduced to 0 near the berm height and the depth of closure to prevent sand from being deposited in the zone higher than the berm height and the beach from being eroded in the zone deeper than the depth of closure using the procedure given by Uda et al. (2013).

Table 1. Calculation conditions.

Wave conditions	Incident waves: $H_I = 0.5$ m, $T = 4$ s Wave direction $\theta_W = +17.5^\circ$ (N17.5°W)
Tide level	M.S.L. 0.0 m
Berm height	$h_R = 1.1$ m
Depth of closure	$h_c = 4H$ (H : wave height at a local point)
Equilibrium slope	$\tan \beta_c = 1/7$
Coefficients of sand transport	Coefficient of longshore sand transport $K_s = 2 \times 10^{-3}$ Coefficient of sand transport by Ozasa and Brampton term $K_2 = 1.62 K_s$ Coefficient of cross-shore sand transport $K_n = 0.2 K_s$
Mesh sizes	$\Delta x = \Delta y = 5$ m
Time intervals	$\Delta t = 1.2$ hr
Total time steps	1×10^4 steps (500 days)
Boundary conditions	8,760
Calculation of wave field	Energy balance equation (Mase, 2001) • Term of wave dissipation due to wave breaking: Dally et al. (1984) model • Wave spectrum of incident waves: directional wave spectrum density obtained by Goda (1985) • Total number of frequency components $N_F = 1$ • Number of directional subdivisions $N_\theta = 8$ • Directional spreading parameter $S_{max} = 2$ • Coefficient of wave breaking $K = 0.17$ and $\Gamma = 0.3$ • Imaginary depth between depth h_0 and berm height h_R : 0.5 m • Lower limit of h in terms of wave decay Φ due to wave breaking: $(h)_{min} = 0.5$ m • Wave energy = 0 where $Z \geq h_R$

Calculation conditions

Referring to the wave observation results between June 2011 and January 2012 measured offshore of Dainikaiho island, as shown in Fig. 1, we assumed a mean significant wave height in this observation period of $H_i = 0.5$ m ($T = 4$ s). The wave direction and directional spreading parameter S_{max} (Goda, 1985) were determined using a trial and error method, so that the measured and calculated shoreline configurations were in good agreement, taking the predominant wave direction of NNW into account. The adopted best-fit wave direction and S_{max} were $N17^\circ W$ and $S_{max} = 2$, respectively. The berm height was assumed to be $h_R = 1.1$ m, as obtained in the field observation on June 11, 2011, and the depth of closure was assumed to be $h_c = 4H$, where H is the local wave height. The equilibrium slope and the slope of the angle of repose were assumed to be $1/7$ and $1/2$, respectively. The calculation domain was discretized by a mesh with intervals of 5 m ($\Delta x = \Delta y = 5$ m). As the initial topography, the sand bar topography measured on July 19, 2011 was assumed. Because only the shoreline position was measured in the observation, a uniform beach with a foreshore slope of $1/7$ was assumed between heights of 1.1 and -2 m.

Calculation results

Figure 13 shows the calculation results. Although the initial sand bar on July 19 had a 50 m width and protruded northward by 100 m, two protrusions had formed on both sides of the sand bar by August 19 owing to the wave action from $N17^\circ W$. The calculation result that a small embayment on the eastern foot of the sand bar was enclosed by the sand spit is in agreement with the observed shoreline. However, there is some discrepancy between the measured and observed shorelines in that the measured shoreline is straight on the west side of the sand bar, whereas the calculated shoreline has a small protrusion. By September 14, the shoreline of the north part of the sand bar significantly retreated with a large inclination toward the east. Furthermore, the shoreline on the east side was connected by a smooth line with a small hollow. By October 14, the shoreline on the north side had markedly retreated and a sand spit had begun to form on the east side. By November 10, the sand spit had elongated and became connected to the other shore, resulting in the formation of a gradually curved shoreline because of the continuous sand supply from the upcoast. The protruding sand bar had eroded to form a gradually curving shoreline by December 21, 2011. Thus, the changes in the sand bar that was formed by the tsunami after the 2011 Great East Japan Earthquake were well predicted using the BG model. Also, the subsequent deformation of the sand bar was found to be due to the action of waves incident from the direction of $N17^\circ W$.

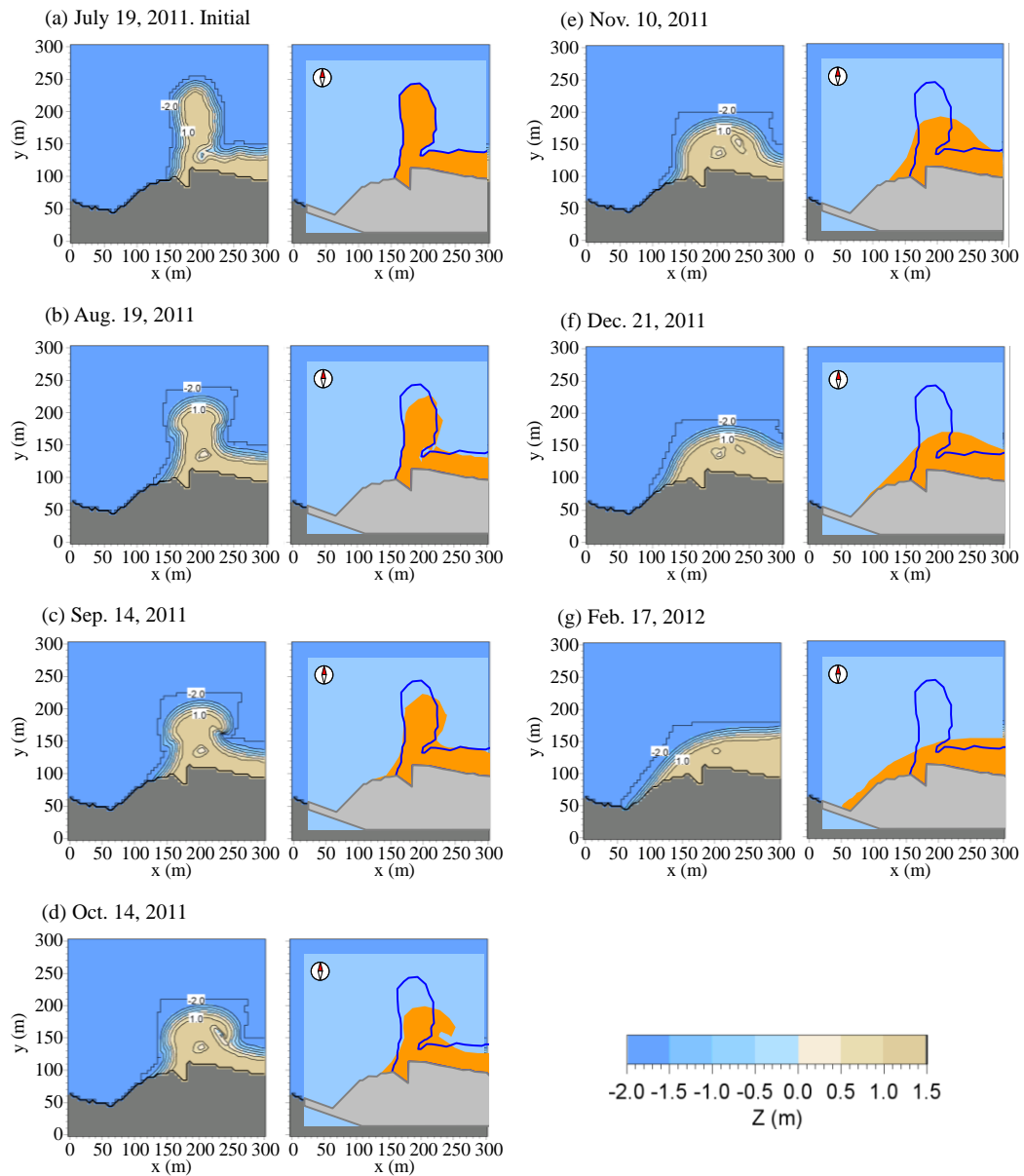


Figure 13. Calculation results of deformation of sand bar.

CONCLUSIONS

The change in the crescent-shaped sand bar offshore of the cusped foreland formed by the overflow of the tsunami after the 2011 Great East Japan Earthquake and subsequent shoreline changes due to wind waves were investigated by field observation. Immediately after the tsunami, the seawall was exposed to waves and was almost destroyed. The seawall, however, was buried again by sand and no further measures were required. These topographic changes were investigated using the BG model. The predicted and measured topographic changes of the crescent-shaped sand bar were in good agreement. The BG model was effectively used to analyze the cause of the beach erosion in front of the seawall, and the wider applicability of the BG model to predicting the deformation of a sand bar has been demonstrated. In addition, further applications to the calculation of the elongation of a sand spit under various conditions are summarized by Uda et al. (2012).

REFERENCES

Dally, W. R., Dean, R. G. and Dalrymple, R. A. 1984. A model for breaker decay on beaches, *Proc. 19th ICCE*, pp. 82-97.

- Goda, Y. 1985. *Random Seas and Design of Maritime Structures*, University of Tokyo Press, Tokyo, 323 p.
- Mase, H. 2001. Multidirectional random wave transformation model based on energy balance equation, *Coastal Eng. J., JSCE*, Vol. 43, No. 4, pp. 317-337.
- Ozasa, H. and Brampton, A. H. 1980. Model for predicting the shoreline evolution of beaches backed by seawalls, *Coastal Eng.*, Vol. 4, pp. 47-64.
- Serizawa, M. and Uda, T. 2011. Prediction of formation of sand spit on coast with sudden change using improved BG model, *Coastal Sediments '11*, pp. 1907-1919.
- Uda, T. and Kanda, Y. 1995. Beach erosion of Futtsu Point in Chiba Prefecture, *Coastal Eng. J., JSCE*, Vol. 42, pp. 651-655. (in Japanese)
- Uda, T., Serizawa, M. and Miyahara, S. 2012. BG model based on Bagnold's concept and its application to analysis of elongation of sand spit and shore - normal sand bar (Chap. 16), pp. 339-374, in 'Numerical Simulation - From Theory to Industry' Andriychuk, M. ed., INTEC.
<http://www.intechopen.com/books/numerical-simulation-from-theory-to-industry/bg-model-based-on-bagnold-s-concept-and-its-application-to-analysis-of-elongation-of-sand-spit-and-s>
- Uda, T., Gibo, M., Ishikawa, T., Miyahara, S., San-nami, T. and Serizawa, M. 2013. Change in carbonate beach triggered by construction of a bridge on Irabu Island and its simulation using BG model, *Asian and Pacific Coasts 2013, Proc. 7th International Conf.*, pp. 24-31.